Check for updates

Energy Technology
Generation, Conversion, Storage, Distribution
www.entechnol.de

Performance Analysis and Optimization of Solar Thermochemical Water-Splitting Cycle with Single and Multiple Receivers

Vishnu Kumar Budama, Stefan Brendelberger, Martin Roeb, and Christian Sattler*

Solar thermochemical water-splitting cycle models for hydrogen production with single and multiple receivers working between 1773 and 1173 K are developed. The receiver pressures and aperture sizes are optimized for maximum cycle efficiency. The efficiency of the cycle increases with the number of receivers because of the decrease in vacuum pump work. The solar-to-fuel efficiency is increased by 14% going from a one receiver system to a four-receiver system. The performance analyses of the cycles with varying direct normal irradiance (DNI) shows that the advantage of multiple receivers vanishes as DNI decreases because of the constant radiation losses from the receiver apertures. These radiation losses from the aperture can be lowered when a receiver with a variable aperture size is used. The efficiency of a two-receiver system increases by 48% at DNI 300 W m^{-2}% and 15% at DNI 900 W m^{-2} using a variable aperture size. The performance of the multireceiver systems with variable aperture size is discussed using a linear regression model. In addition, the option of cogeneration of hydrogen and electricity in a multireceiver system is analyzed. The efficiencies of single-, two-, three-, and four-receiver systems for cogeneration are 19.6%, 20.0%, 20.57%, and 21.1%, respectively.

1. Introduction

Fossil fuels have been the primary source of energy in the 20th century for power generation, transportation, and industrial purposes.[1,2] The emissions from the combustion of fossil fuels have a substantial role in global warming and the earth's temperatures may reach an unacceptable level if this trend continues.[3] One crucial step to reduce emissions and mitigate global warming is moving to carbon-neutral fuels, like hydrogen. Hydrogen can be used in internal combustion engines as a heat source and in fuel cells for electricity generation.[4] The possibility to produce hydrogen with renewable energy and its high gravimetric energy density are the two prime advantages of hydrogen fuel.[5] Currently, more than 95% of the global hydrogen is produced using fossil fuels and therefore causes CO_2 emissions.[6] Hydrogen produced from a low cost and environmentally friendly technology is essential to address future global warming problems.

Water electrolysis using renewable electricity, steam reforming of biogas, and solar thermochemical water splitting are promising hydrogen production methods from renewable energy sources.[7–16] Solar thermochemical water-splitting technology has the potential for scale-up and commercialization of hydrogen production to meet future energy demands.[17] In a two-step thermochemical water-splitting process, a redox material goes through a cycle of thermal reduction and oxidation reactions to produce hydrogen fuel.[18–23] Thermal reduction is an endothermic reaction, whereas oxidation is an exothermic reaction. The first thermochemical water-splitting cycle was proposed by Nakamura in 1977 using Fe_3O_4/3Feo as redox material.[24]

The hydrogen yield from the thermochemical cycle directly depends on the extent of reaction/reduction of redox material in the reduction step.[25] High temperature and low partial pressure of oxygen in the reduction chamber are the two requirements to achieve a high extent of reduction.[26] The high-temperature requirement is met by solar thermal irradiation in a solar thermochemical water-splitting cycle. Mechanical vacuum pumps and inert gas sweeping are the two available approaches to maintain low oxygen pressure in the reduction chamber.[27] Less energy-intensive methods for oxygen removal during reduction are under development.[27–29] Reheating the inert gas and separating oxygen from the inert gas are the two limitations in the inert gas sweeping approach.[30] High mechanical energy consumption and high costs, especially at low pressures, are significant limitations in the case of mechanical vacuum pumps. The drop in efficiency of the vacuum pumps at low pressures leads to high mechanical energy requirements if the reduction chamber is operated at low pressure.[31] The vacuum pump work demand can significantly impact the overall solar-to-fuel conversion efficiency. This limitation was addressed using a cascading pressure reactor where the thermal reduction happens in multiple stages successively at low pressures.[32–36] This enables the

V. K. Budama, S. Brendelberger, M. Roeb, C. Sattler
Deutsches Zentrum für Luft- und Raumfahrt/German Aerospace Center – DLR
Institut for Future Fuels
51147 Köln, Germany
E-mail: Vishnu.budama@dlr.de

The ORCID identification number(s) for the author(s) of this article can be found under https://doi.org/10.1002/ente.202100220.

© 2021 The Authors. Energy Technology published by Wiley-VCH GmbH. This is an open access article under the terms of the Creative Commons Attribution-NonCommercial-NoDerivs License, which permits use and distribution in any medium, provided the original work is properly cited, the use is non-commercial and no modifications or adaptations are made.

DOI: 10.1002/ente.202100220

thermochemical cycle to run at lower pressures compared with a single-stage receiver. Ermanoski concluded, that the oxygen partial pressure during reduction can be reduced by more than an order of magnitude using a pressure cascade, yielding significant efficiency gains.[32] The study carried out by Brendelberger et al. showed an 66% pumping work reduction compared with a single reactor design if a six-chamber system is used.[35]

A study on different pumping options in a thermochemical cycle was done by Brendelberger et al.[27] The compatibility of mechanical pumps, jet pumps, and thermochemical pumps is evaluated considering energy efficiency and economics. The equivalent heat demand by a mechanical pump is significantly lower compared with the heat required by a jet pump (considering 40% heat to electricity conversion efficiency). From a parasitic power demand perspective, operating pressures are expected to be limited to values in the range of 80 Pa for mechanical pumps and 2000 Pa for jet pumps. On the other side, jet pumps are the more economical solution, and cost considerations of mechanical pumps are likely to limit the reasonable pressure region to higher values. An interesting alternative is thermochemical pumps, as presented by Brendelberger et al.[27,28] Their efficiency can be significantly higher than the mechanical and jet pumps at low pressures (especially below 100 Pa), but this technology is still under development.[27,28] Another promising approach was presented by Ermanoski and Stechel and demonstrated by Xu et al.,[29,37] which is based on a thermally driven adsorption/desorption cycle. Also, this technology is at an early development stage.

This work includes evaluating and comparing the performance of solar thermochemical cycles using single-stage and multistage reduction. Mechanical vacuum pumps inlet pressure-dependent efficiencies are considered for this study. The optimum receiver pressure and aperture size are calculated for single- and multireceiver systems for maximum efficiency of the cycle. The efficiencies of single- and multistage receivers (up to four) are calculated using a model written in Python, and the performance values are compared. The properties of Ceria are used in this model, but this approach can be used for other materials as well by substituting corresponding material properties. The efficiency of each model is evaluated at different direct normal irradiance (DNI) values, and annual average efficiencies are estimated.

2. System Description

A model of a solar thermochemical water-splitting systems for hydrogen production with single and multiple receivers is developed and optimized. The system consists of a solar receiver–reactor and a water-splitting reactor for reduction and oxidation reactions, respectively. The system includes several auxiliary components to support the reactions and to enhance the performance of the cycle. This model considered Ceria particles as redox material for the thermodynamic analysis of the cycle. The complete configuration of single- and multi-receiver models with all the components and their purpose is discussed in this section.

2.1. Single Receiver Model

The configuration of a single-receiver solar thermochemical water-splitting system is shown in **Figure 1**. The system includes a solar receiver that acts as a thermal reduction reactor to reduce redox particles. The particles are heated to the targeted reduction temperature and reduced in the solar receiver using solar radiation from the solar field. A vacuum pump is used to maintain low pressure in the receiver by continuously removing the oxygen released due to the reduction of particles. The released oxygen from the receiver is cooled before reaching the pump to decrease the vacuum pump work. A solid–solid particle recuperator and a steam generator are used to cool the particles to the designed reoxidation temperature before entering the water-splitting reactor. The reduced particles exit the receiver at high temperature and exchange heat with the oxidized particles at low temperature exiting from the water-splitting reactor. The particles are further cooled to the reoxidation temperature of particles in the steam generator, and this heat is used to generate high-temperature steam. The high-temperature steam generated in the steam generator is used for hydrogen production in the water-splitting reactor, and the excess steam can be recovered. The particles are reoxidized using steam in the water-splitting reactor and produce hydrogen. The oxidized particles exiting the water-splitting reactor absorb heat from the hot particles in the recuperator and enter the solar receiver for the next cycle. The steam–hydrogen mixture leaves the water-splitting reactor and enters the hydrogen separator, where hydrogen is separated from steam. The extracted hydrogen is compressed and stored using a hydrogen pump. A water pump is used to supply water to the steam generator to produce high-temperature steam using the sensible heat of the particles. The mass and energy balance calculations were done for all the components of the system at an instantaneous DNI input value onto the solar field. The equations used for the thermodynamic analysis of the system are described in the following sections. The temperature, and specific enthalpy of ith stream is represented as T_i, h_i.

The solar radiation supplied to the solar receiver is utilized for two purposes in a thermochemical cycle: as sensible heat to raise the temperature of the particles to the reduction temperature and as chemical energy for the thermal reduction of the particles. The radiation losses from the receiver aperture are calculated using the average of the fourth power of the particle temperature in the solar receiver and aperture size.[20] The total radiation supplied to the receiver $(\dot{Q}_2)$ is given in Equation (1), and radiation losses are given in Equation (2).

$$\dot{Q}_2 = \dot{n}_\mathrm{p} \cdot (C_\mathrm{p,p} \cdot (T_3 - T_7) + (h_3 - h_7)) \tag{1}$$

$$\dot{Q}_\mathrm{rad,loss} = \sigma \cdot A_\mathrm{apr} \cdot \left(\left(\frac{T_3^4 + T_7^4}{2} \right) - T_\mathrm{amb}^4 \right) \tag{2}$$

where $\dot{n}_\mathrm{p}$ is the particle flow rate in the cycle, $C_\mathrm{p,p}$ is the specific heat of the particles at constant pressure, $\dot{Q}_\mathrm{rad,loss}$ are the radiation heat losses from the aperture, σ is the Stefan–Boltzmann's constant, A_apr is the area of the aperture, and T_amb is the atmospheric temperature.

The extent of thermal reduction and the enthalpy for the reduction (Δh) are calculated using the Equation (3) and (4) given by Bulfin et al.[38]

© 2021 The Authors. Energy Technology published by Wiley-VCH GmbH

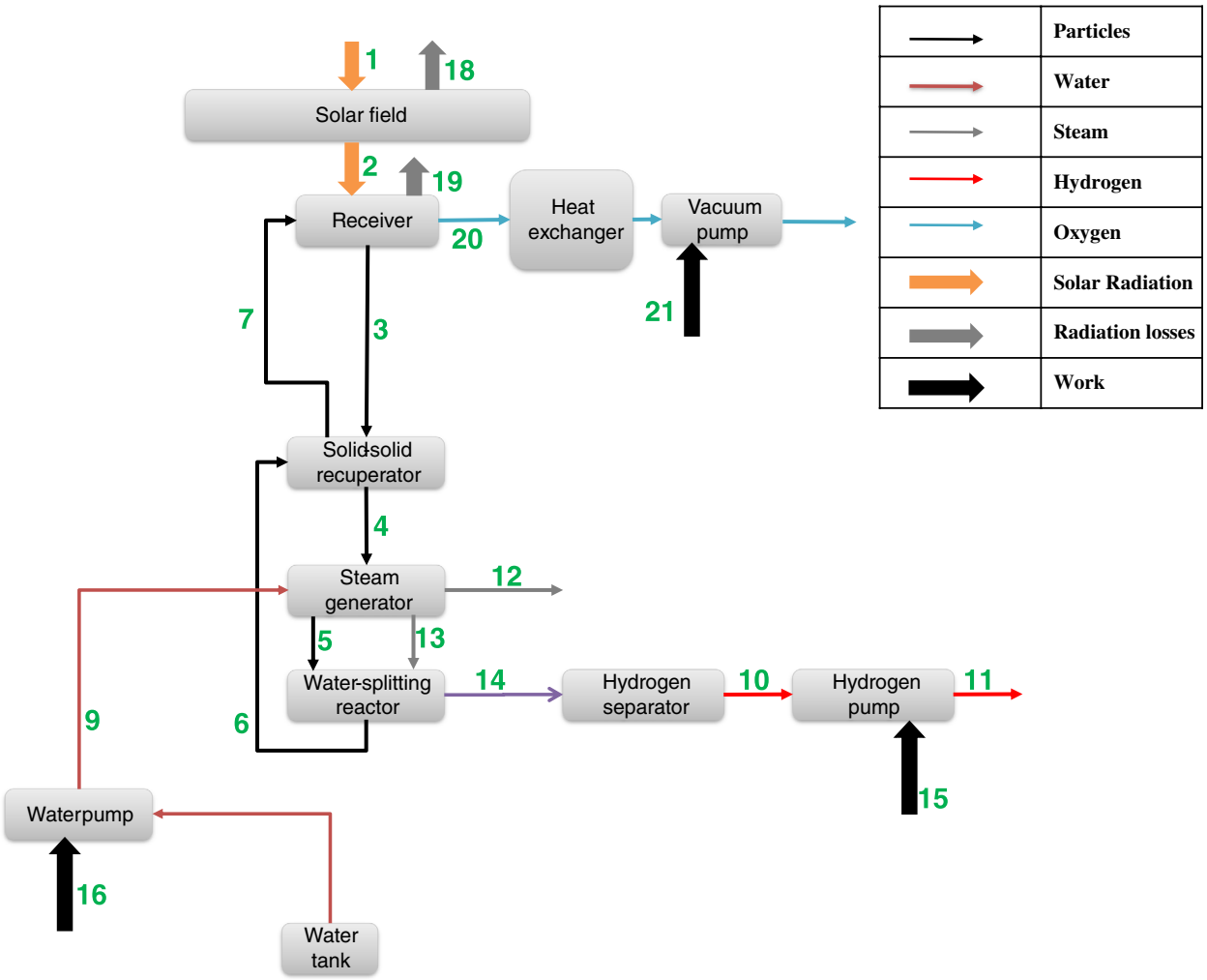

Figure 1. Configuration of a single-receiver solar thermochemical water-splitting system.

$$\left(\frac{\delta_{red}}{0.35-\delta_{red}}\right) = 8700 \cdot P_{O_2}^{-0.217} \cdot \exp\left(\frac{-195.6}{R \cdot T_{red}}\right) \quad (3)$$

$$\Delta h = 478 - 1158 \cdot \delta + 1790 \cdot \delta^2 + 23368 \cdot \delta^3 - 64929 \cdot \delta^4 \quad (4)$$

The required solar radiation onto the solar field is calculated using the total heat supplied to the receiver and the efficiency of the solar field (η_{SF}), as shown in Equation (5). The area of the solar field (A_{SF}) is calculated using the total radiation required at a DNI as given in Equation (6)

$$\dot{Q}_1 = \frac{\dot{Q}_2 + \dot{Q}_{rad,loss}}{\eta_{SF}} \quad (5)$$

$$A_{SF} = \frac{\dot{Q}_1}{DNI} \quad (6)$$

The reduced hot particles from the receiver enter the recuperator at reduction temperature, and cold particles enter at oxidation temperature. The total heat transfer rate in the recuperator and exit temperatures depends on the recuperator's effectiveness, as shown in Equation (7)–(10).

$$\dot{Q}_{rec} = \varepsilon_{rec} \cdot \dot{Q}_{max} \quad (7)$$

$$\dot{Q}_{max} = \dot{n}_p \cdot C_{p,p} \cdot (T_3 - T_6) \quad (8)$$

$$T_4 = T_3 - \frac{\dot{Q}_{rec}}{\dot{n}_p \cdot C_{p,p}} \quad (9)$$

$$T_7 = T_6 + \frac{\dot{Q}_{rec}}{\dot{n}_p \cdot C_{p,p}} \quad (10)$$

where $\dot{Q}_{rec}$ is the actual heat transfer, ε_{rec} is the effectiveness of the recuperator, and $\dot{Q}_{max}$ is the maximum possible heat transfer (heat transfer if the exit temperature of the cold particles is equal to the inlet temperature of the hot particles).

The effectiveness of the recuperator controls the exit temperature of the particles, and thus the hot particles have to be cooled further. Hence, a steam generator is used to cool the particles till

© 2021 The Authors. Energy Technology published by Wiley-VCH GmbH

the reoxidation temperature. The molar flow rate of water is calculated such that the particles are always cooled to the reoxidation temperature. The energy balance equation of the steam generator is given in Equation (11).

$$\dot{Q}_{sg} = \dot{n}_w \cdot (\dot{q}_{wat} + \dot{q}_{lat} + \dot{q}_{st}) \tag{11}$$

where $\dot{Q}_{sg}$ is total heat transfer rate in the steam generator, $\dot{n}_w$ is the molar flow rate of water, $\dot{q}_{wat}$ is the heat required to raise a mole of water from inlet to saturation temperature, $\dot{q}_{lat}$ is latent heat per mole of water, and $\dot{q}_{st}$ is the heat required to raise a mole of steam from saturation to exit temperature.

The molar hydrogen production rate $(\dot{n}_{hyd})$ in the water-splitting reactor is calculated using Equation (12). The effectiveness of the reoxidation reaction (ε_{ox}) is the ratio between reduction and actual reoxidation extents to that of reduction and equilibrium reoxidation extents (δ_{ox}^{eq}).[20]

$$\dot{n}_{hyd} = \varepsilon_{ox} \cdot \dot{n}_p \cdot (\delta_{red} - \delta_{ox}) \tag{12}$$

$$\varepsilon_{ox} = \frac{\delta_{red} - \delta_{ox}}{\delta_{red} - \delta_{ox}^{eq}} \tag{13}$$

where δ_{red} is the final extent of reduction of particles at the exit of the receiver, and δ_{ox} is the extent of reduction after the reoxidation reaction.

The heat equivalent of the mechanical work consumed by the vacuum pump, water pump, and hydrogen pump are given in Equation (14)–(16).

$$\dot{W}_{21} = \frac{\dot{n}_{20} \cdot R \cdot T_{20} \cdot \ln(P_{vp})}{\eta_{vp} \cdot \eta_{hm}} \tag{14}$$

$$\dot{W}_{15} = \frac{\dot{n}_{10} \cdot R \cdot T_{10} \cdot \ln(P_{hp})}{\eta_{hp} \cdot \eta_{hm}} \tag{15}$$

$$\dot{W}_{16} = \frac{\rho_{wat} \cdot g . H_{loss} \cdot \dot{V}_9}{\eta_{wp} \cdot \eta_{hm}} \tag{16}$$

$$\dot{W}_{tot} = \dot{W}_{21} + \dot{W}_{15} + \dot{W}_{16} \tag{17}$$

where R is the universal gas constant, η_{vp}, η_{hp}, and η_{wp} are the efficiencies of the vacuum pump, hydrogen pump, and water pump, respectively, P_{vp} and P_{hp} are pressure ratios in vacuum pump and hydrogen pump, ρ_{wat} is the density of water, H_{loss} is total head loss (pressure loss) of water in the system, $\dot{V}_9$ is the volumetric flow rate of water, and η_{hm} is the heat to mechanical efficiency.

The solar-to-fuel efficiency (η_{SF}), is equal to the ratio of rate hydrogen energy produced to the sum of solar radiation input $(\dot{Q}_1)$ to the solar field and heat equivalent auxiliary work in the cycle. The rate of hydrogen energy produced is calculated using the higher calorific value (HHV) of hydrogen at standard temperature and pressure conditions (STP). The equation for the solar-to-fuel efficiency is given in Equation (18).

$$\eta_{SF} = \frac{(\dot{n}_{hyd} \cdot \mathrm{HHV})}{\dot{Q}_1 + \dot{W}_{tot}} \tag{18}$$

2.2. Multireceiver Model

The rate of hydrogen production from a thermochemical cycle directly depends on the extent of thermal reduction of particles in the solar receiver (reduction chamber). The extent of thermal reduction (δ_{red}) is a function of the partial pressure of oxygen (P_{O_2}) in the receiver and the temperature of the particles (T_{red}), as shown in Equation (3). The work consumed by the vacuum pump to maintain a low pressure in the receiver will have a significant impact on the cycle efficiency. The work required by the vacuum pump increases sharply as pressure approaches low vacuum pressures in the receiver because the efficiency of the vacuum pump decreases at low pressures. For the model, a multistage vacuum pump system outlined in the study by Brendelberger et al.[39] is considered. The dependency of vacuum pump efficiency on the inlet pressure for this system is shown in **Figure 2**.

The steep fall in the efficiency of the vacuum pump significantly impacts the efficiency of the thermochemical cycle at low pressures. This limitation can be addressed using cascading pressure receivers where the thermal reduction happens staged in multiple receivers. A series of reduction chambers are used in

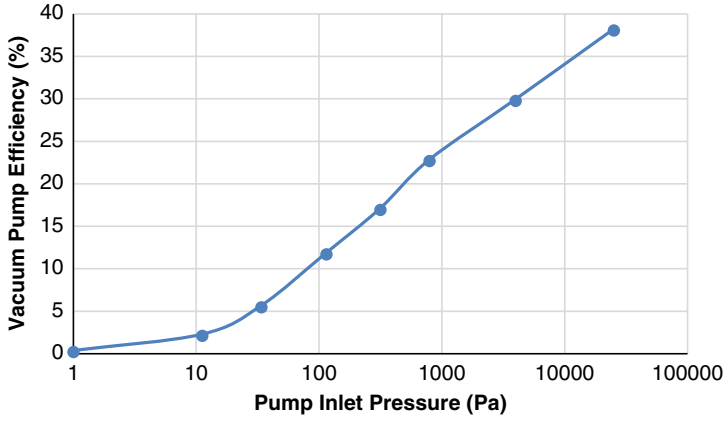

Figure 2. Vacuum pump efficiency as a function of the inlet pressure (derived from values presented in the study by Brendelberger et al.[39]).

© 2021 The Authors. Energy Technology published by Wiley-VCH GmbH

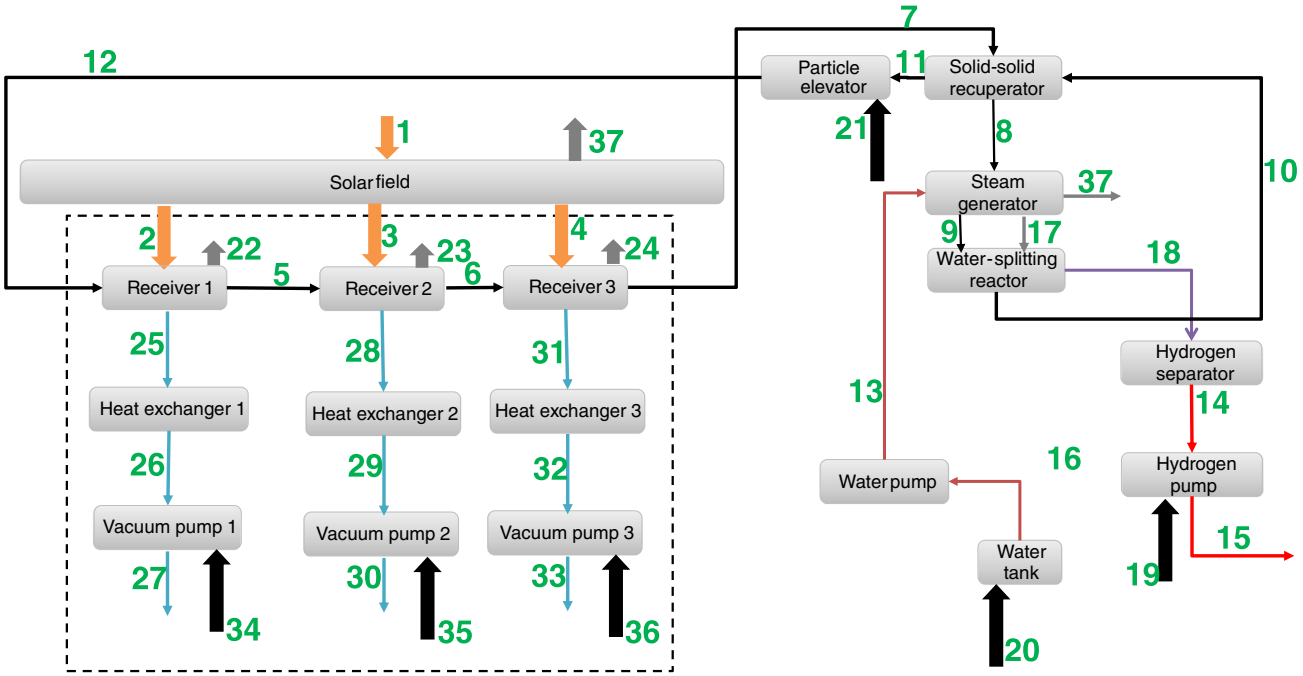

Figure 3. Configuration of a multireceiver system of a solar thermochemical water-splitting system.

a multi-receiver model operating at successively lower pressures. This helps to reduce the total vacuum pump work for the same total extent of reduction. The particles are partially reduced in each receiver and reach the target extent of reduction in the final receiver. The configuration of a multi-receiver model with three reduction chambers, as an example of a multi-receiver system, is shown in **Figure 3**. The equations used for the multi-receiver models are similar to a single receiver model.

3. Input Values

The system's instantaneous performance is analyzed at 1000 W m^{-2} DNI and a molar particle flow rate of 500 mol s^{-1}. The reduction temperature is kept at 1800 K, and receiver operating pressure and aperture size are optimized for maximum efficiency of the cycle. The temperature difference between the reduction and oxidation reactions is considered as 600 K to minimize the water requirement during the water-splitting reaction.[40] The area of the solar field is calculated using constant DNI 1000 W m^{-2}. The solar field efficiency increases as the flux density at the aperture decreases, and a linear interpolation is used to estimate the solar field efficiency at any given flux density. The annual average efficiencies of the solar field of 61.9% at a flux density of 2.2 MW m^{-2}, and 53.1% at 4.5 MW m^{-2} are taken from Pitz-Paal.[41] An average specific heat value is assumed for particles at all chemical states and temperatures. The total hydraulic pressure loss in the system's water circuit is estimated as 10 bar to calculate the water pump work. The higher calorific value of the hydrogen fuel at STP conditions is 285 830 J mol^{-1}. **Table 1** shows the parameters for the baseline analysis of a single-receiver system at the design point.

Table 1. Input parameters for the baseline analysis of single- and multireceiver systems.

Parameter	Value	Units
Universal gas constant (R)	8.3144621	J mol^{-1} K^{-1}
Stefan–Boltzmann's constant	5.670373×10^{-8}	W/m^{-2} K^{-4}
Ambient temperature	298.15	K
Ambient pressure	101 325	Pa
Molecular weight of Ceria	172	g mol^{-1}
Effectiveness of recuperator	0.7	–
Thermal conductivity of insulation material[42]	0.15	W m K^{-1}
Heat-to-mechanical energy conversion efficiency	40	%
Average specific heat of Ceria particles[43]	80	J mol^{-1}
Average specific heat of the water	76	J mol^{-1}

4. Results

The performance of single- and multireceiver thermochemical water-splitting systems is studied to optimize receiver pressures and aperture sizes. The solar-to-fuel conversion of the cycle depends on the receiver pressure, vacuum pump work, radiation losses from the aperture, and efficiency of the solar field, and therefore, all the parameters are considered simultaneously for the optimization. The area of the solar field is calculated at constant instantaneous DNI input of 1000 W m^{-2}. The decrease in receiver pressure leads to an increase in hydrogen production and vacuum pump work as well. Therefore, the receiver pressure is to be optimized for maximum solar-to-fuel efficiency of the cycle. The radiation losses from the aperture increase if the

© 2021 The Authors. Energy Technology published by Wiley-VCH GmbH

aperture size is increased at a constant temperature. The interdependency of each parameter indicates that both the receiver pressure and flux density are to be optimized concurrently.

The model calculates the efficiency of the cycle for every possible combination of receiver pressure and flux density. The input values to the optimization model are a range of receiver pressures (10–100 000 Pa) with an interval of 10 Pa and flux densities (2.2–4.5 MW m^{-2}) with an interval of 0.1 MW m^{-2} for the first iteration. The radius of the aperture is calculated using energy demand and flux density. The output of the first iteration is a combination of receiver pressure and flux density for which the solar-to-fuel efficiency of the cycle is maximum. The input values for the next iteration are from −20% to +20% of the receiver pressure and flux density, for which the efficiency is maximum in the previous iteration. The interval size decreases in every iteration, for example, 1 Pa in the second iteration here. The iterations are continued till the efficiency converges (difference between the two iterations is less than 0.01 %). The size of the solar field and aperture radius is calculated for every individual receiver pressure and flux density.

4.1. Single-Receiver System

The optimum receiver pressure and aperture radius are 60 Pa and 1320 mm, respectively, for the maximum efficiency of 11.15% for a single-receiver system. The radiation flux density at the optimized efficiency is 2.5 MW m^{-2}, and the hydrogen production rate is 11.19 mol s^{-1}. **Figure 4** shows the variation of solar-to-fuel efficiency for receiver pressures from 10 to 500 Pa at a fixed flux density of 2.5 MW m^{-2}. The efficiency of the cycle is 8.0% at 10 Pa, whereas the hydrogen production rate is 51% higher compared with hydrogen production at an optimized pressure of 60 Pa. This shows the significant effect of vacuum pump work on the efficiency of a thermochemical cycle. The vacuum pump work and radiation losses decrease with an increase in receiver pressure and lead to better efficiency of the system. The relation between receiver pressure, efficiency, and aperture size in a single-receiver system is shown in Figure 4. The size of the aperture decreases as the receiver pressure increases because of the decrease in energy demand to the receiver. The efficiency of the system initially increases as receiver pressure increases because of decreasing vacuum pump work up to 60 Pa, and then efficiency decreases as pressure increases because of a drop in hydrogen production rate. This is in line with the operating pressure limits reported by Brendelberger et al.[36] The output values of the single-receiver system at optimized receiver pressure and flux density are shown in **Table 2**.

4.2. Multireceiver System

A multireceiver model is similar to a single-receiver model but considers multiple receivers operating at different pressures. The redox particles are partially reduced in the first receiver and then enter the next receiver operating at a lower pressure compared with the previous receiver, and the particles are further reduced. The operating pressure of each receiver and the size of each receiver aperture are to be optimized for maximum efficiency in a multireceiver system. The optimization technique is similar to a single-receiver system, where the efficiency of the cycle is calculated for all possible combinations of receiver pressures and flux densities.

The maximum efficiency of a two-receiver system is 11.89%, and the hydrogen production rate is 12.16 mol s^{-1}. The receiver pressures are 318 and 54 Pa in receivers 1 and 2, respectively, and aperture radii are 1226 and 504 mm for receivers 1 and 2, respectively. The efficiency of a two-receiver system is 7% higher than a single-receiver system. The hydrogen production rate increases because the optimized receiver pressure in receiver 2 (54 Pa) is lower than the optimized operating pressure in the single-receiver system. The heat supplied to the two solar receivers is not the same as the particles are heated and reduced in the first receiver and only reduced in the second receiver. Hence, the heat supplied to the first receiver is 11.56 and 2.03 MW to the second receiver.

The temperature of the particles in each receiver impacts the extent of thermal reduction, radiation losses, and vacuum pump work, indicating that the operating temperature in each receiver

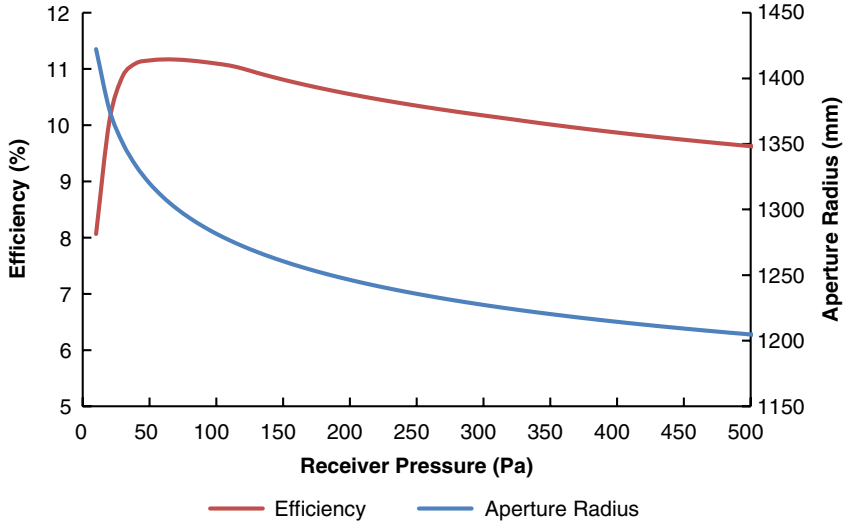

Figure 4. Single-receiver cycle efficiency with varying receiver pressure and aperture radius at constant DNI.

© 2021 The Authors. Energy Technology published by Wiley-VCH GmbH

Table 2. Performance results of single- and multireceiver systems.

Parameter	Single	Two	Three	Four	Units
Solar-to-fuel efficiency	11.17	11.89	12.34	12.74	%
Receiver pressure	60	318	887	3050	Pa
		54	106	1912	
			31	96	
				30	
Hydrogen production rate	11.91	12.16	13.57	13.66	mol/s
Aperture radius	1310	1226	1172	1121	mm
		504	550	60	
			447	674	
				431	
Radiation losses	2.39	2.09	1.91	1.75	MW
		0.43	0.51	0.01	
			0.34	0.48	
				0.31	
Total	2.39	2.52	2.76	2.55	
Vacuum pump work (heat equivalent)	4.06	0.95	0.44	0.20	MW
		1.5	0.89	0.01	
			1.8	1.42	
				1.78	
	Total	2.45	3.13	3.41	
Radiation from solar field	26.1	22.41	20.48	18.75	MW
		4.05	4.21	0.06	
			3.23	4.97	
				3.09	
	Total	26.46	27.92	26.87	
Efficiency of the solar field	60.75	60.94	60.94	60.94	%
		60.60	61.90	60.18	
			60.45	60.18	
				60.18	
Area of the solar field	26 100	22 407	20 481	18 751	m^2
		4053	4206	59	
			3231	4971	
				3089	
Total	26 100	26 460	27 918	26 690	

is another optimization parameter in a multireceiver system. The effect of the temperature of particles in each receiver is analyzed for a two-receiver system. The exit temperature from the first receiver is named as the intermediate temperature in a two-receiver system. The efficiency of the system is calculated for a range of intermediate temperatures keeping the receiver pressures and aperture sizes constant at optimized values. The effect of intermediate temperature on the work consumed by the two vacuum pumps and efficiency is shown in **Figure 5**. The vacuum pump work of the first receiver increases as the intermediate temperature increases because of the increase in oxygen release rate. The oxygen release rate and vacuum pump work decrease in the second receiver as the intermediate temperature increases because the final reduction temperature is fixed. Nevertheless, the total vacuum pump work decreases, and efficiency increases as the intermediate temperature increases, as shown in Figure 5. The efficiency of the system is maximum, when the intermediate temperature is 1800 K, and this is true for any combination of receiver pressures and aperture sizes. Therefore, the operating temperature of the receivers is not considered for optimization in multireceiver models in this study and is kept constant in all receivers.

A similar optimization technique is used to optimize the performance of three- and four-receiver systems. The maximum efficiencies of three- and four-receiver systems are 12.34% and 12.74%, respectively. The efficiency increases with each receiver and a four-receiver system giving 15% higher efficiency than a single-receiver system, but the gains are diminishing. If inter receiver heat losses of the particles or heat losses through the insulation of the receiver would be considered in the model, the establishment of an optimum number of receivers would be expected. The performance results of single- and multireceiver systems at the optimized receiver pressures and flux densities are shown in Table 2.

4.3. Sensitivity Analysis

The efficiencies of single- and multireceiver systems with varying DNI levels are analyzed at fixed receiver pressures and aperture

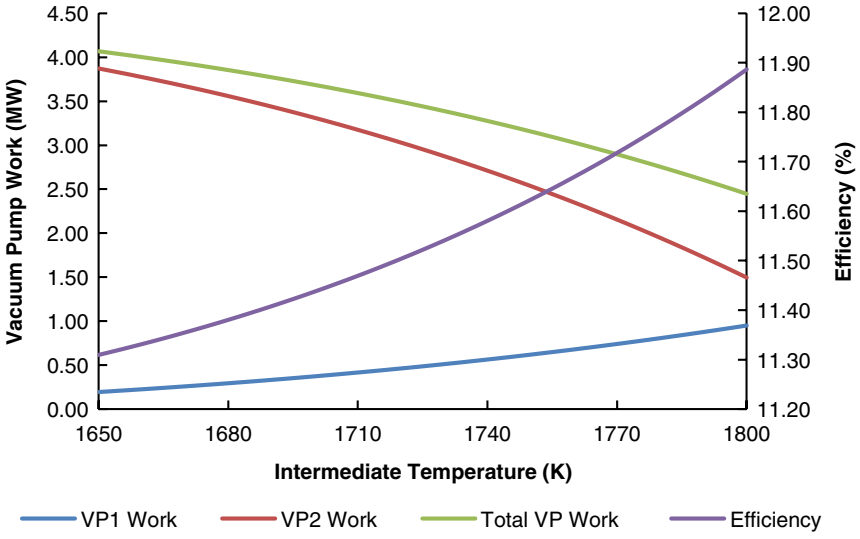

Figure 5. Effect of intermediate temperature on vacuum pump work and efficiency of a two-receiver system.

© 2021 The Authors. Energy Technology published by Wiley-VCH GmbH

sizes. The change in DNI varies the heat input to the receiver, and the particle flow rate varies accordingly. The efficiencies of single- and multireceiver systems is decreasing as DNI decreases, as shown in **Figure 6**. It is evident from the figure that the difference between the efficiency of single- and multireceiver systems narrowing as DNI decreases. There is no significant difference between the efficiencies of the single- and four-receiver systems at 300 W m^{-2} DNI. Though the percentage difference is same at all DNI values, the quantitative difference leads to a significant drop in hydrogen production. This indicates that the benefit of a multireceiver system is reducing as DNI decreases. One of the reasons for this is that the radiation losses from the receivers do not vary with DNI because the temperature and aperture sizes are fixed. The efficiency of the multireceiver systems can be increased at low DNI values by reducing the radiation losses. This can be achieved with a variable aperture receiver in which the size of the aperture can be changed during the operation. The aperture size can be decreased at low DNI levels since the energy demand from the receiver is lowered. The performance analysis of a multireceiver system with varying aperture size is analyzed in this section.

The effect of variable aperture sizes on the efficiency of a two-receiver system is shown in **Figure 7**. The efficiency of the system is calculated for a range of aperture sizes for every DNI value from 300 to 900 W m^{-2}. Figure 7 shows that the advantage of the variable aperture is significant at low DNI levels, and the

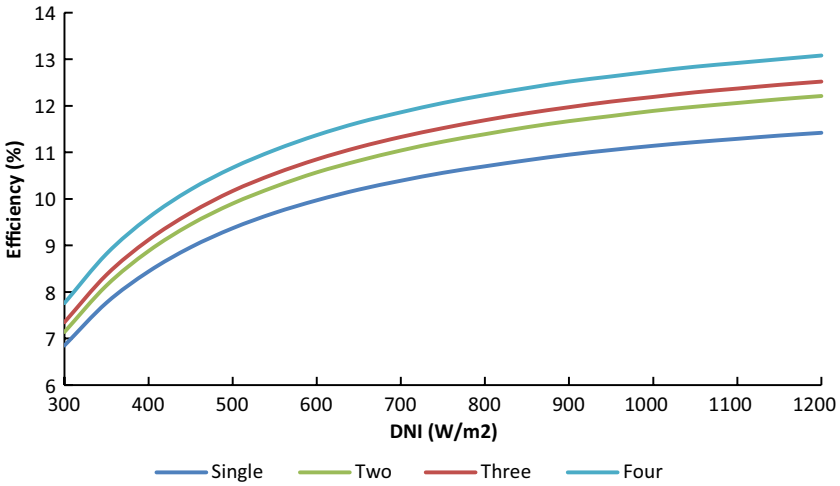

Figure 6. Dependency of efficiencies of single- and multi-receiver systems with varying DNI.

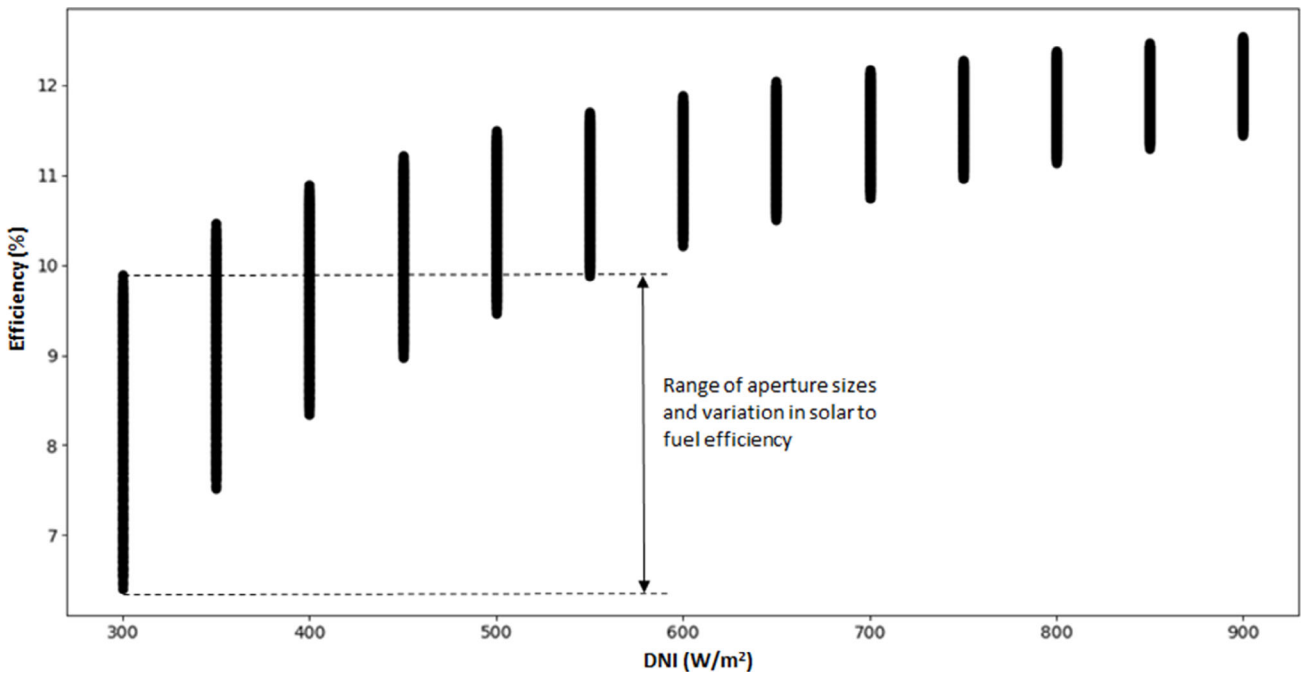

Figure 7. Range of solar-to-fuel efficiencies for variation in aperture size.

© 2021 The Authors. Energy Technology published by Wiley-VCH GmbH

effect drops as DNI increases. The range of aperture sizes is selected such that the flux density is always between 1 and 2.2 MW m^{-2}. There is ≈48% rise in efficiency at DNI 300 W m^{-2} for a two-receiver system, which signifies the advantage of variable aperture, and this requires an increase in flux density.

A linear regression model is used to predict the advantage of variable aperture in a multireceiver solar thermochemical cycle. The efficiency of the system is calculated for a range of aperture sizes (within mentioned flux densities) for every DNI value between 300 and 900 W m^{-2}. The efficiency is calculated for ≈0.4 million combinations, and this sample set is used for the linear regression model. The results of the linear regression model are shown in Equation (19)–(21). These equations can be used to predict the efficiency of the multireceiver system at any given DNI level and aperture sizes.

$$\eta_{SF2} = 13.539 + 0.0057305 \cdot \mathrm{DNI} - 0.005006 \cdot R_{21} - 0.0018481 \cdot R_{22} \tag{19}$$

$$\eta_{SF3} = 12.506 + 0.0093182 \cdot \mathrm{DNI} - 0.006169 \cdot R_{31} - 0.000019 \cdot R_{32} - 0.000005 \cdot R_{33} \tag{20}$$

$$\eta_{SF4} = 10.202 + 0.01277 \cdot \mathrm{DNI} - 0.0054201 \cdot R_{41} - 0.000156 \cdot R_{42} - 0.000742 \cdot R_{43} - 0.00046714 \cdot R_{44} \tag{21}$$

where η_{SF2}, η_{SF}, and η_{SF4} indicates the efficiencies of two-, three-, and four-receiver systems, R_{ij} indicates the aperture radius corresponding to the i number of receiver system and jth receiver.

The aforementioned equations are valid in the DNI range 300–900 W m^{-2}. The range for R_{21}, R_{31}, and R_{41} is 900–1300 mm. R_{22} range is 400–504 mm, R_{32} range is 400–581 mm, R_{33} is 300–447 mm, R_{42} the range is 100–160 mm, R_{43} range is 520–674 mm, and R_{44} is 300–431 mm.

4.4. Variable Aperture at Constant DNI

The significant impact of aperture size and radiation losses on the efficiency of the cycle is discussed in the previous sections. The real-time conditions in the solar field and unforeseen losses in the field may lead to variation in theoretically estimated solar field efficiency. The variable aperture receiver can help in this scenario to minimize the losses and maximize efficiency. The change in solar field efficiency with varying flux density is not considered in this analysis. In this section, a logistic regression model is used to predict the tolerable limits of the aperture sizes in multireceiver systems.

The efficiency of the system is calculated for more than 71 000 combinations of receiver pressures and aperture sizes for a two-receiver system. The range of receiver pressures is 100–500 Pa for receiver 1 and 10–100 Pa for receiver 2. The range of aperture sizes for receivers 1 and 2 is 1100–1400 and 400–600 mm. The efficiency of the system for every combination is compared with the maximum efficiency (11.17%) of a single-receiver system. The efficiency of the two-receiver system is better than a single-receiver system in 90% of the combinations. Therefore, it can be concluded that a two-receiver system will have a better performance than a single-receiver system for several combinations of receiver pressures and aperture sizes. This allows modifying the aperture size and operating pressure in real-time conditions within a range and still benefits the advantage of the multireceiver system. The advantage in efficiency is not the same with every combination of receiver pressure and aperture size. Therefore, a logistic regression model is developed to predict the advantage in efficiency for any particular combination of receiver pressure and aperture size. The results of the logistic regression analysis for a two-receiver system compared with a single receiver system are given in Equation (20). The value $(X_{2,1})$ calculated from Equation (22) is substituted in Equation (23) to predict the probability, $P(\eta_2 > \eta_1)$.

$$X_{2,1} = -0.0002 \cdot P_{21} + 0.3411 \cdot P_{22} - 0.0034 \cdot R_{21} - 0.0029 \cdot R_{21} \tag{22}$$

$$P(\eta_2 > \eta_1) = \frac{1}{1 + e^{-X_{2,1}}} \tag{23}$$

P_{21}, and P_{22} represents pressures in receivers 1 and 2, and $P(\eta_2 > \eta_1)$ is the probability of a two-receiver system being better than a single-receiver system for a particular combination of receiver pressures and aperture size.

The probability above 0.5 indicates that the two-receiver system will have better efficiency than a single-receiver system for that particular combination of receiver pressures and aperture sizes. As the probability value approaches unity, it represents the efficiency of the system is approaching maximum efficiency. The combinations of receiver pressures and aperture sizes that give a probability of less than 0.5 should not be considered for designing a two-receiver system. Therefore, the logistic regression model is useful for choosing a wide range of combinations of receiver pressures and aperture sizes for which the efficiency of a two-receiver system is better than a single-receiver system.

The logistic regression analysis is carried out for a three-receiver system similar to a two-receiver system. The three-receiver system's efficiency is calculated for little more than a million combinations of receiver pressures and aperture sizes. The efficiency of a three-receiver system for every combination of receiver pressures and aperture sizes is compared with the maximum efficiency of a two-receiver system (11.89%). There are ≈67% of the cases where the efficiency of a three-receiver system is better than a two-receiver system. The results of the logistic regression model of a three-receiver system compared with a two-receiver system are shown in Equation (22) and (23). These equations can be used to choose the operating parameters of a three-receiver system without losing the advantage of the third receiver.

A three-receiver system designed with optimized aperture sizes 1172, 550, and 447 mm and optimized pressures 887, 106, and 31 Pa, respectively, gives a probability of 0.97 using Equation (24) and (25). If the system is designed with aperture sizes 1350, 650, and 550 mm and keeping the receiver pressures unchanged, then the probability is 0.93. This indicates that the system with the changed aperture sizes is better than a two-receiver system (because the probability is more than 0.5), and the efficiency is less than maximum efficiency because it is less than 0.97.

© 2021 The Authors. Energy Technology published by Wiley-VCH GmbH

$$X_{3,2} = 0.0041 \cdot P_{31} - 0.0008 \cdot P_{32} + 0.0565 \cdot P_{33} - 0.0012 \cdot R_{31} - 0.0003 \cdot R_{32} - 0.0015 \cdot R_{33} \quad (24)$$

$$P(\eta_3 > \eta_2) = \frac{1}{1 + e^{-X_{3,2}}} \quad (25)$$

where $P(\eta_3 > \eta_2)$ is the probability of a three-receiver system having more efficiency compared with a two-receiver efficiency.

4.5. Annual Average Efficiency

The annual average efficiencies of the single- receiver and multiple receiver systems are calculated using the hourly DNI data at Ouarzazate, Morocco. The calculated annual average efficiencies and annual hydrogen production are shown in **Table 3**. The DNI levels above 300 $W m^{-2}$ are considered for the annual performance calculations and at fixed aperture size. The annual hydrogen production increases with an increase in the number of receivers, as shown in Table 3.

4.6. Coproduction of Electricity

Coproduction of electricity is a promising way to increase the overall system performance. The thermochemical cycle is operated at high temperature, requiring high concentration factors, which results in high spillage losses. If a hybrid receiver design is used, to make use of parts of the spillage and if this heat and the waste heat of the process are used to produce electricity, the overall system performance can be significantly improved.[21] A preliminary study on the option of coproduction of electricity in a multireceiver system is discussed in this section. The potential of electricity coproduction is more in the case of the multireceiver system as there are several receivers operating at high temperatures. The intercept efficiency, which accounts for spillage losses at the entrance of the aperture, is ≈85%.[41] It is assumed that 50% of these losses can be recovered and converted to electrical energy. The excess steam recovered from the steam generator is another source to generate electricity in a solar thermochemical cycle. The combined hydrogen and electrical efficiency of the plant are estimated based on the above two heat recovery options. The combined efficiencies of single-, two-, three-, and four-receiver models are 19.6%, 20.0%, 20.57%, and 21.1%, respectively, showing improvement potential. This approach should be further investigated in more detail.

Table 3. Annual average efficiency and annual hydrogen production for single- and multireceiver systems.

No. of receivers in the system	Annual average efficiency [%]	Annual hydrogen production [Ton]
One	10.18	195.59
Two	10.81	200.24
Three	11.10	218.40
Four	11.62	224.92

5. Conclusion

The performance of a solar thermochemical water-splitting system with different numbers of solar receivers is analyzed, and the system parameters are optimized. Thermochemical cycles with one-, two-, three-, and four-receiver systems are studied to optimize system parameters. The operating pressure and temperature of each receiver and size of the aperture are optimized for maximum solar-to-fuel conversion efficiency. In-line with previous studies on multireceiver systems, this study has shown that lower receiver operating pressures can be achieved with cascading pressure chambers. A multireceiver system gives the best efficiency when all the receivers are operated at the final maximum receiver temperature. A single-receiver system gives maximum efficiency at receiver pressure of 60 Pa. The lowest pressures for the multireceiver models are 54, 31, and 30 Pa for two-, three-, and four-receiver systems, respectively. The hydrogen production rate increases with the addition of each receiver because the operating pressure of the final receiver is decreasing. The receiver operating pressures and aperture sizes are simultaneously optimized for maximum solar-to-fuel efficiency of the cycle for each system. An empirical correlation between solar field efficiency and flux density at the aperture is used, and the size of the solar field is estimated.

The efficiencies of single- and multireceiver systems are calculated for a range of DNI levels from 300 to 1200 $W m^{-2}$. The efficiency of multireceiver systems decreases rapidly compared with a single-receiver system as DNI decreases because of constant radiation losses irrespective of DNI level because the area of the aperture is the same. A solar receiver with variable aperture size can be used to minimize the radiation losses and increase cycle efficiency at low DNI levels. A linear regression model is used to predict the efficiency of the cycle at any given DNI and aperture sizes. The efficiency of a two-receiver system is increased by ≈48% with a variable aperture compared with a fixed aperture size. The advantage of a variable aperture at constant DNI is also discussed. The uncertainties in the solar field lead to higher losses than analytically predicted and may require a different aperture size for better efficiency of the system. Therefore, the receiver operating pressures have also to be different for maximum cycle efficiency. A logistic regression model is used to predict the tolerable limits of receiver operating pressures and aperture sizes for the best performance of the system. The equation developed using the logistic regression model calculates the probability of having better efficiency of a three-receiver system compared with a two-receiver system. Similar equations can be developed to compare the performance of any multireceiver systems. The option of electricity coproduction is introduced in a multireceiver solar thermochemical cycle, and an efficiency of up to 21.1% for the coproduction is predicted. The annual average performance of single- and multireceiver systems is calculated using hourly DNI data at Ouarzazate, Morocco. The experimental validation of the improvement potential for the multireceiver approach is work in progress. Further detailed analysis on cogeneration of electricity, considering the kinetics of chemical reactions, and technoeconomic analysis can give deeper insights on the performance of multireceiver solar thermochemical water-splitting cycles.

© 2021 The Authors. Energy Technology published by Wiley-VCH GmbH

Acknowledgements

The authors thank the European Union and the State of North Rhine-Westphalia for Co-funding the work via ERDF.NRW Investment for Growth and Employment (EFRE-0801589). Also, supported by the Federal Ministry for Economic Affairs and Energy on the basis of a decision by the German Bundestag (03EIV221).

Open access funding enabled and organized by Projekt DEAL.

Conflict of Interest

The authors declare no conflict of interest.

Data Availability Statement

The data that supports the findings of this study are available in the supplementary material of this article.

Keywords

hydrogen fuels, multireceiver models, thermochemical cycles, solar water splitting

Received: March 22, 2021
Revised: July 6, 2021
Published online:

[1] J. O. Abe, A. P. I. Popoola, E. Ajenifuja, O. M. Popoola, *Int. J. Hydrogen Energy* **2019**, *44*, 15072.
[2] E. De Cian, I. S. Wing, *Nota di Lav.* **2016**, *16*.
[3] S. Bilgen, *Renew. Sustain. Energy Rev.* **2014**, *38*, 890.
[4] M. Balat, *Int. J. Hydrogen Energy* **2008**, *33*, 4013.
[5] P. P. Edwards, V. L. Kuznetsov, W. I. F. David, N. P. Brandon, *Energy Policy* **2008**, *36*, 4356.
[6] Z. Wang, R. R. Roberts, G. F. Naterer, K. S. Gabriel, *Int. J. Hydrogen Energy* **2012**, *37*, 16287.
[7] I. Dincer, C. Acar, *Int. J. Hydrogen Energy* **2014**, *40*, 11094.
[8] S. Haussener, C. Xiang, J. M. Spurgeon, S. Ardo, N. S. Lewis, A. Z. Weber, *Energy Environ. Sci.* **2012**, *5*, 9922.
[9] E. Cetinkaya, I. Dincer, G. F. Naterer, *Int. J. Hydrogen Energy* **2012**, *37*, 2071.
[10] P. Zhai, S. Haussener, J. Ager, R. Sathre, K. Walczak, J. Greenblatt, T. Mckone, *Energy Environ. Sci.* **2013**, *6*, 2380.
[11] S. Haussener, S. Hu, C. Xiang, A. Z. Weber, N. S. Lewis, *Energy Environ. Sci.* **2013**, *6*, 3605.
[12] C. Agrafiotis, M. Roeb, C. Sattler, *Renew. Sustain. Energy Rev.* **2015**, *42*, 254.
[13] L. Xiao, S. Y. Wu, Y. R. Li, *Renew. Energy* **2012**, *41*, 1.
[14] T. Wiltowski, K. Mondal, A. Campen, D. Dasgupta, A. Konieczny, *Int. J. Hydrogen Energy* **2008**, *33*, 293.
[15] C. Acar, I. Dincer, *Int. J. Hydrogen Energy* **2014**, *39*, 15362.
[16] F. Suleman, I. Dincer, M. Agelin-Chaab, *Int. J. Hydrogen Energy* **2016**, *41*, 8364.
[17] D. Yadav, R. Banerjee, *Renew. Sustain. Energy Rev.* **2016**, *54*, 497.
[18] A. Steinfeld, *Int. J. Hydrogen Energy* **2002**, *27*, 611.
[19] A. Steinfeld, *Sol. Energy* **2005**, *78*, 603.
[20] V. K. Budama, N. G. Johnson, A. McDaniel, I. Ermanoski, E. B. Stechel, *Int. J. Hydrogen Energy* **2018**, *43*, 17574.
[21] V. K. Budama, N. G. Johnson, I. Ermanoski, E. B. Stechel, *Int. J. Hydrogen Energy* **2021**, *46*, 1656.
[22] A. Bayon, A. de la Calle, K. K. Ghose, A. Page, R. McNaughton, *Int. J. Hydrogen Energy* **2020**, *45*, 12653.
[23] A. de la Calle, A. Bayon, *Int. J. Hydrogen Energy* **2019**, *44*, 1409.
[24] T. Nakamura, *Sol. Energy* **1977**, *19*, 467.
[25] M. Lange, M. Roeb, C. Sattler, R. Pitz-Paal, *Int. J. Hydrogen Energy* **2015**, *40*, 12108.
[26] I. Ermanoski, N. P. Siegel, E. B. Stechel, *J. Sol. Energy Eng.* **2013**, *135*, 031002.
[27] S. Brendelberger, H. von Storch, B. Bulfin, C. Sattler, *Sol. Energy* **2017**, *141*, 91.
[28] S. Brendelberger, J. Vieten, M. Roeb, C. Sattler, *Int. J. Hydrogen Energy* **2019**, *44*, 9802.
[29] I. Ermanoski, E. B. Stechel, *Sol. Energy* **2019**, *198*, 578.
[30] S. Brendelberger, M. Roeb, M. Lange, C. Sattler, *Sol. Energy* **2015**, *122*, 1011.
[31] S. Brendelberger, J. Felinks, M. Roeb, C. Sattler, in *Analysis of Reduction Step for Thermochemical Redox Cycles. Thermochemical Knowledge for Tomorrow*.
[32] I. Ermanoski, *Int. J. Hydrogen Energy* **2014**, *39*, 13114.
[33] I. Ermanoski, J. Grobbel, A. Singh, J. Lapp, S. Brendelberger, M. Roeb, C. Sattler, J. Whaley, A. McDaniel, N. P. Siegel, *AIP Conf. Proc.* **2016**, *1734*.
[34] S. Brendelberger, C. Sattler, *Sol. Energy* **2015**, *113*, 158.
[35] S. Brendelberger, M. Roeb, C. Sattler, *ES2014-6421 Solid Phase Heat Recovery and Multi Chamber Reduction for Redox Cycles*, **2014**, pp. 1–9.
[36] A. Singh, J. Lapp, J. Grobbel, S. Brendelberger, J. P. Reinhold, L. Olivera, I. Ermanoski, N. P. Seigel, A. McDaniel, M. Roeb, C. Sattler, *Sol. Energy* **2017**, *157*, 365.
[37] M. Xu, I. Ermanoski, E. B. Stechel, S. Deng, *Chem. Eng. J.* **2019**, *389*, 124026.
[38] B. Bulfin, F. Call, M. Lange, O. Lübben, C. Sattler, R. Pitz-Paal, I. V. Shvets, *Energy Fuels* **2015**, *29*, 1001.
[39] S. Brendelberger, A. Rosenstiel, A. Lopez-Roman, C. Prieto, C. Sattler, *Int. J. Hydrogen Energy* **2020**, *45*, 26104.
[40] I. Ermanoski, *Energy Proc.* **2015**, *69*, 1731.
[41] R. Pitz-Paal, N. B. Botero, A. Steinfeld, *Sol. Energy* **2011**, *85*, 334.
[42] M. S. Al-Homoud, *Build. Environ.* **2005**, *40*, 353.
[43] M. Mogensen, N. M. Sammes, G. A. Tompsett, *Solid State Ionics* **2000**, *129*, 63.

© 2021 The Authors. Energy Technology published by Wiley-VCH GmbH